Environmental Research 193 (2021) 110564

Contents lists available at ScienceDirect

Environmental Research

journal homepage: www.elsevier.com/locate/envres

Ibuprofen degradation using a Co-doped carbon matrix derived from peat as a peroxymonosulphate activator

Zhongfei Ren [a,*], Henrik Romar [b], Toni Varila [b,c], Xing Xu [d], Zhao Wang [i], Mika Sillanpää [e,f,g,h], Tiina Leiviskä [a]

[a] Chemical Process Engineering, University of Oulu, P.O. Box 4300, FIN-90014, University of Oulu, Oulu, Finland
[b] Research Unit of Sustainable Chemistry, University of Oulu, P.O. Box 4300, FIN-90014, University of Oulu, Oulu, Finland
[c] Applied Chemistry, Kokkola University Consortium Chydenius, University of Jyvaskylä, P.O. Box 567, FI-67101, Kokkola, Finland
[d] Shandong Key Laboratory of Water Pollution Control and Resource Reuse, School of Environmental Science and Engineering, Shandong University, Jinan, 250100, PR China
[e] Institute of Research and Development, Duy Tan University, Da Nang, 550000, Viet Nam
[f] Faculty of Environment and Chemical Engineering, Duy Tan University, Da Nang, 550000, Viet Nam
[g] School of Civil Engineering and Surveying, Faculty of Health, Engineering and Sciences, University of Southern Queensland, West Street, Toowoomba, 4350, QLD, Australia
[h] Department of Chemical Engineering, School of Mining, Metallurgy and Chemical Engineering, University of Johannesburg, P. O. Box 17011, Doornfontein, 2028, South Africa
[i] School of Chemical and Metallurgical Engineering, University of the Witwatersrand, 2050 Johannesburg, South Africa

ARTICLE INFO

Keywords:
Ibuprofen
Advanced oxidation process
Cobalt oxides
Carbon-based catalyst
Pharmaceuticals and personal care products

ABSTRACT

The wider presence of pharmaceuticals and personal care products in nature is a major cause for concern in society. Among pharmaceuticals, the anti-inflammatory drug ibuprofen has commonly been found in aquatic and soil environments. We produced a Co-doped carbon matrix (Co–P 850) through the carbonization of Co^{2+} saturated peat and used it as a peroxymonosulphate activator to aid ibuprofen degradation. The properties of Co–P 850 were analysed using field emission scanning electron microscopy, energy filtered transmission electron microscopy and X-ray photoelectron spectroscopy. The characterization results showed that Co/Fe oxides were generated and tightly embedded into the carbon matrix after carbonization. The degradation results indicated that high temperature and slightly acidic to neutral conditions (pH = 5 to 7.5) promoted ibuprofen degradation efficiency in the Co–P 850/peroxymonosulphate system. Analysis showed that approx. 52% and 75% of the dissolved organic carbon was removed after 2 h and 5 h of reaction time, respectively. Furthermore, the existence of chloride and bicarbonate had adverse effects on the degradation of ibuprofen. Quenching experiments and electron paramagnetic resonance analysis confirmed that $SO_4^{\cdot-}$, ·OH and $O_2^{\cdot-}$ radicals together contributed to the high ibuprofen degradation efficiency. In addition, we identified 13 degradation intermediate compounds and an ibuprofen degradation pathway by mass spectrometry analysis and quantum computing. Based on the results and methods presented in this study, we propose a novel way for the synthesis of a Co-doped catalyst from spent NaOH-treated peat and the efficient catalytic degradation of ibuprofen from contaminated water.

1. Introduction

Over the last decade, an increasing number of studies have shown that various pharmaceuticals and personal care products (PPCPs) are found in surface water, ground water and wastewater (Hasan et al., 2016). The widespread contamination of PPCPs poses a threat to ecosystems as well as to human health. Owing to their low aqueous solubility and degradation resistance, PPCPs tend to accumulate in aquatic organisms and may cause various problems even at very low concentrations. PPCP contamination originates from pharmaceutical wastewater, human excretion and improper discharge. Due to their unclear influence on the environment and on humans, most PPCPs have been recognized as emerging contaminants (ECs) and have become a cause for major concern (Zhang et al., 2019).

* Corresponding author.
E-mail address: zhongfei.ren@oulu.fi (Z. Ren).

https://doi.org/10.1016/j.envres.2020.110564
Received 31 August 2020; Received in revised form 23 November 2020; Accepted 27 November 2020
Available online 2 December 2020

Ibuprofen (IBU), a mass-produced non-steroidal anti-inflammatory drug, generally used for relieving pain, fever and inflammation, is attracting great attention due to its potential harmful impact on humans and the persistent contamination of aquatic and soil ecosystems. IBU and its metabolites from human and animal excretion can end up in natural waters and soils, as conventional wastewater treatment lines typically do not have a separate pharmaceutical degradation process (Saeid et al., 2018; Sousa et al., 2018). Due to the extensive usage of IBU, it has been detected in surface water and sewage effluents at ng/L and μg/L levels (Archer et al., 2017; Deblonde et al., 2011; Mailler et al., 2015). A study on the seasonal variation of pharmaceutical concentrations in surface water conducted in eastern Finland showed that IBU concentration detected in the Rakkolanjoki river was up to 1830 ng/L (Meierjohann et al., 2016). Other studies showed that up to 5291 ng/L, 1317 ng/L and 17,600 ng/L of ibuprofen were detected in Spain, Portugal and South Africa, respectively (Gumbi et al., 2017; Paíga et al., 2016; Robles-Molina et al., 2014). Although the concentration is at a low level, the potential risk to the ecosystem from constant exposure needs consideration. Therefore, it is important to prevent ibuprofen and other PPCPs from entering the environment by developing feasible techniques for wastewater treatment.

To date, several removal techniques have been used to eliminate ibuprofen contamination from water, such as adsorption (Z. Li et al., 2019b), ozonation (Ikhlaq et al., 2014), biodegradation, photodegradation (Gu et al., 2019), membrane separation (Williams et al., 2012) and advanced oxidation processes (AOPs) (Saeid et al., 2018). Among these, AOPs have been widely investigated and applied for degradation of PPCPs from an aqueous environment owing to their high efficiency, non-selectivity and straightforward operation. In conventional AOPs, highly reactive oxidizing radicals, i.e. hydroxyl radicals (E^o = 2.8 V), can be generated by photo, ultrasound or catalyst activation (Ghanbari and Moradi, 2017). In addition, sulphate radical-based AOPs have aroused increasing interest over the last decade. Compared to hydroxyl radicals, sulphate radicals show a preference for electron transfer reactions. Hydroxyl radicals tend to participate in various reactions with equal preference, which means that a sulphate radical has a higher half-life (30–40 μs) than a hydroxyl radical (20 ns) (Ghanbari and Moradi, 2017; Rastogi et al., 2009). Besides, the higher oxidation potential (E^o = 2.5–3.1 V) and stability of the sulphate radical make it more effective for the degradation of a recalcitrant organic pollutant (Rastogi et al., 2009; Yanan et al., 2020). The oxidants used to generate sulphate radicals usually contain persulphate ($S_2O_8^{2-}$, PS) and peroxymonosulphate (HSO_5^-, PMS) (Duan et al., 2020; Shang et al., 2019). For example, one kind of oxidant, $2KHSO_5{\cdot}KHSO_4{\cdot}K_2SO_4$, which contains peroxymonosulphate (also known as Oxone) has been widely used for the degradation of organics since it is more stable and convenient than H_2O_2 (Shi et al., 2012). Transition metal ions such as Cu^{2+}, Mn^{2+}, Ni^{2+}, Fe^{2+} and Co^{2+} and their oxides coupled with PMS could accelerate sulphate radical generation and hence improve degradation performance for organic pollutants (Chen et al., 2019; Duan et al., 2019; Wang and Wang, 2018). The cobalt ion has been proven to have the highest catalytic efficiency for PMS activation, and has been studied for various organic pollutants (Anipsitakis et al., 2006; Chen et al., 2017; Shi et al., 2012). However, cobalt leaching in the Co/PMS system presents a major drawback, which hinders its application (Peng et al., 2021). Therefore, many studies have turned to the use of cobalt oxides, which are supported by or bundled with diverse materials to reduce cobalt leaching and improve catalytic performance. For instance, in the study by Shi et al. (2012), 0.2 mM Orange II was totally decomposed within 6 min with 0.1 g/L Co_3O_4-decorated graphene oxide and 2 mM PMS, with only slight ion leaching. Tian et al. (2018) fabricated Co core@N–S co-doped C-shell nanoparticles that exhibited high degradation performance. In their study, 20 mg/L p-hydroxybenzoic acid was completely removed within 45 min (PMS: 6.5 mM, catalyst dosage: 0.066 g/L). However, some of the supporting materials, such as graphene oxide (GO), reduced graphene oxide (rGO) and carbon nanotubes (CNTs), are expensive (Ghanbari and Moradi, 2017). In contrast, we found that the use of biomaterials as a catalyst precursor is more economic and environmentally friendly. However, there is limited information available on research into bio-based catalysts. Complicated synthesis methods, high energy cost and harmful waste generation may limit the application of bio-based catalysts. Therefore, it is necessary to develop an eco-friendly synthesis method that meets green chemistry requirements.

Peat, an abundant biomaterial found in water-logged and marshy land, consists of lignin, cellulose and organic acids, making it an ideal material to provide a carbon matrix for catalyst doping. Thanks to their excellent properties, peat char-supported metal catalysts have been used for syngas generation and oxygen evolution reaction in the energy sector (Teppor et al., 2020; Wang et al., 2020). Peat can also be used as a biosorbent to remove metals and organic pollutants from water (Chiou et al., 2000; Gogoi et al., 2018; Ho and McKay, 2000). However, the disposal of spent biosorbent remains a challenging issue, especially when it has been used for metal adsorption. To avoid secondary pollution from the spent biosorbent, it is important to develop ways to reuse the spent sorbent. In this study, we propose a novel way to fabricate a peat-derived Co-doped carbon matrix to activate peroxymonosulphate for ibuprofen degradation. This is a creative solution for the disposal problem and enables full utilization of the spent peat biosorbent. We chose NaOH-treated peat (NaOH–P) with a high metal cation adsorption capacity (Leiviskä et al., 2018) as the raw material to adsorb Co^{2+} from water. We then carbonized the Co-loaded peat at four different temperatures to obtain carbon-based catalysts doped with cobalt oxides. This was then applied for IBU degradation with PMS as oxidant. X-ray photoelectron spectroscopy (XPS), transmission electron microscopy (TEM) and scanning electron microscopy (SEM) were used to analyse the structure and components of the catalysts. The surface area and pore size distribution were also measured. We investigated the effects of dosage, pH, temperature and contact time to determine the optimal operating conditions for degradation. The degradation intermediates of IBU were analysed by liquid chromatography–mass spectrometry (LC-MS), and quantum computing was used to investigate the degradation mechanism and pathway.

2. Materials and methods

2.1. Chemical reagents

Cobalt nitrate hexahydrate ($Co(NO_3)_2{\cdot}6H_2O$), sodium hydroxide (NaOH), sulphuric acid (H_2SO_4, 98%), hydrochloric acid (HCl), sodium chloride (NaCl), sodium bicarbonate ($NaHCO_3$), sodium phosphate (Na_3PO_4), potassium nitrate (KNO_3), methanol, Oxone ($2KHSO_5{\cdot}KHSO_4{\cdot}K_2SO_4$), 5,5-dimethyl-1-pyrroline-N-oxide (DMPO), 2,2,6,6-Tetramethyl-4-piperidone (4-oxo-TEMP), ethanol (EtOH), tert-butyl alcohol (TBA), p-benzoquinone (p-BQ) and L-histidine (L-his) were provided by Sigma-Aldrich. Ibuprofen (IBU) was provided by Thermo Fisher. All of the reagents used in this study were of analytical reagent grade. Milli-Q water was used for the preparation of samples and solutions unless otherwise stated.

2.2. Preparation of Co-loaded carbon catalysts from NaOH-treated peat (NaOH–P)

Peat was obtained from Stora Enso Veitsiluoto pulp mill (Finland). The pre-treatment methods were the same as reported earlier (Leiviskä et al., 2018). In brief, raw peat was first dried in an oven at 80 °C for 24 h and sieved to obtain a finely-divided fraction of 90–250 μm. Then, 100 g of this peat fraction was added to 2 L of NaOH solution (0.1 M) and mixed for 6 h at 25 °C. The NaOH-treated peat (NaOH–P) was subsequently washed with deionized water until the pH reached neutral, and dried at 80 °C for 24 h.

To fabricate Co-doped carbon catalysts, NaOH–P (25 g) was first soaked in 500 mL of $Co(NO_3)_2$ solution (3.5 g/L Co) at 25 °C with

stirring for 24 h. Then, it was washed with deionized water and dried in an oven at 60 °C for 24 h. The carbonization of cobalt-impregnated NaOH–P was carried out in a N_2 atmosphere in a stainless-steel tube in a tube furnace (Nabertherm RT200/13) at temperatures of 600, 700, 800 and 850 °C for 2 h with a ramping rate of 5 °C/min. Following this, the product was named Co–P X, where X denotes the temperature. After being cooled to room temperature under N_2 flow, the carbonized catalysts were then ground into powder, followed by washing with ethanol and deionized water. Next, all of the samples were dried in an oven at 80 °C and stored before use. The flow chart for catalyst preparation and the catalytic degradation of IBU is shown in Fig. 1.

2.3. IBU degradation experiments

Unless otherwise noted, all of the IBU degradation experiments were carried out using a 400 mL beaker with 10 mg/L IBU solution, 2 mM PMS and 0.1 g/L catalyst at below 23 °C. Firstly, all four products were tested at pH 7.6 (pH 1000L, VWR, Germany). At scheduled intervals, 1 mL of sample was taken by syringe and filtered with a 0.45 μm membrane (VWR, polyethersulphone), after which 0.5 mL of methanol was added to quench the radical reaction. The concentration of residual IBU was determined by high performance liquid chromatography (HPLC) (see section 2.4 on characterization). The concentration of dissolved organic carbon (DOC) was measured using a SIEVERS 900 portable TOC analyser. The samples were filtered through a 0.45 μm membrane (VWR, polyethersulphone) before the DOC measurement.

The effects of pH (3–11), temperature (23 °C, 35 °C and 45 °C), catalyst dosage (0.05 g/L to 0.2 g/L) and PMS dosage (0.5 mM–4 mM) were determined for the catalyst that performed the best. The reusability test was carried out with Co–P 850. After the 1st and 2nd runs, the catalyst was collected by filtration with a 0.45 μm membrane (VWR, polyethersulphone) and washed several times with Milli-Q water before the next run. The influence of co-existing anions (Cl^-, HCO_3^-, $H_2PO_4^-$ and NO_3^-) on IBU degradation performance was also evaluated. Different radical scavengers such as ethanol, tert-Butyl alcohol, p-benzoquinone and L-histidine were introduced to the reaction system to identify the reactive oxygen species (ROS). In addition, the reactive radicals were also analysed using an electron paramagnetic resonance (EPR) spectrometer (CMS-8400) using TEMP and DMPO as trapping reagents.

The kinetics of the IBU catalysis degradation data was fitted by a first-order equation, which is given as follows:

$$\ln\frac{C_t}{C_0} = -Kt + C \quad (1)$$

where C_t is the concentration of IBU (mg/L) at time t, C_0 is the original concentration of contaminants (mg/L), K is the degradation rate constant (1/min) and C is the constant term. The calculated R square values are given in Table S1.

2.4. Characterization

The surface compositions of the carbonized samples were analysed by X-ray photoelectron spectroscopy (XPS) (Thermo Fisher Scientific ESCALAB 250Xi) and X-ray diffraction (XRD) (Rigaku SmartLab 9 kW). The specific surface areas and pore size distributions of the catalysts were calculated from the isotherms obtained from N_2 adsorption, using the Brunauer–Emmett–Teller (BET) method and the Density Functional Theory (DFT) algorithm, assuming slit-formed pores. Before the measurements, the samples were degassed for 3 h in order to clean the surfaces. The measurements were performed using a Micromeritics ASAP 2020 instrument. The morphology, elemental distribution and particle size of Co–P 850 were analysed with an energy filtered transmission electron microscope (EFTEM) (LEO 912 OMEGA) equipped with an Energy-Dispersive X-ray Spectroscopy (EDS) detector (Oxford Instruments, X-Max 80) and field emission scanning electron microscope (FESEM) (Zeiss Sigma). The thermogravimetric analysis of the NaOH-peat sample was conducted under N_2 flow with a ramping rate of 5 °C/min (STA 409 PC).

2.5. Analytical methods and quantum computing

The concentration of IBU was measured by HPLC (Shimadzu HPLC, Japan) at a wavelength of 220 nm with a C18 column (Waters SunFire C18, 5 μm, 4.6 mm × 150 mm). The mobile phase was a mixture of 0.1% formic acid and acetonitrile (25/75, v/v) with a 1 mL/min flow rate under isocratic mode. The injection volume and column temperature were 50 μL and 30 °C, respectively. The UV absorption spectrum and the calibration curve of the ibuprofen solution are shown in Fig. S7 and Fig. S8. The degradation intermediates of IBU were detected by an HPLC ion trap mass spectrometry (MS) system (Thermo Ultimate 3000, Thermo LCQ Fleet, USA). A mixture of methanol and water (60/40) was used as the mobile phase with a 0.2 mL/min flow rate in isocratic mode. The injection volume was 5 μL and the column temperature was 23 °C. MS analysis was carried out in negative ion mode. The temperature and the electrospray ionization potential were 320 °C and 4 kV, respectively. The frontier electron density (FED) calculations of IBU were carried out at the B3LYP/6-311G* level using the Gaussian 09 program (Abbasoglu, 2006).

3. Results and discussion

3.1. Characteristics of the Co-loaded catalysts

The specific surface area (SSA), pore volume, pore size distribution and yield of the carbonized catalyst at different temperatures are shown in Table 1. We found that the carbonization temperature had a significant influence on the SSA and pore size distribution. Co–P 700 had the highest surface area of 409 m^2/g with the highest micropore proportion

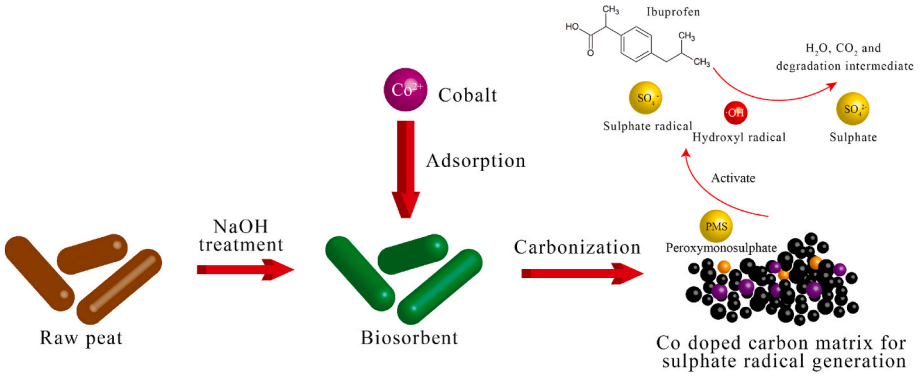

Fig. 1. Flow chart for catalyst preparation and catalytic degradation of IBU.

Table 1
Specific surface area, total pore volume, pore size distribution and yield of the Co-doped carbon catalysts.

Sample	SSA (m^2/g)	Total pore volume (cm^3/g)	Micro-pores (%)	Meso-pores (%)	Macro-pores (%)	Yield (%)
Co–P 600	386	0.133	95	5		38.4
Co–P 700	409	0.136	96.3	3.2	0.5	36.2
Co–P 800	358	0.147	74.8	24.5		35.2
Co–P 850	290	0.156	53.2	46.2		35.0

of 96.3%, whereas the SSA of Co–P 850 dropped to 290 m^2/g along with a decrease in micropore proportion to 53.2%. One possible reason is that the more fragile carbon structure was destroyed at the high carbonization temperature, which turned micropores into mesopores, resulting in a loss of surface area, a significantly higher proportion of mesopores and a slightly higher total pore volume. This explanation was supported by the TGA analysis of NaOH–P (Fig. S1), which showed a continuous decrease in NaOH–P mass as the carbonization temperature (600 °C–850 °C) increased.

Fig. 2 shows the FESEM images of Co–P 850. The images show two typical surface structures, an uneven surface with trenches (Fig. 2b) and a porous surface with a rough frame (Fig. 2c and d). A clear change is visible before and after carbonization when comparing the FESEM image of NaOH-treated peat (Leiviskä et al., 2018) to that of the carbonized sample (Fig. 2). Most of the biomass was burned and removed during the carbonization process, whereas the supporting frame was carbonized and thus remained.

Further investigation on the microstructure of Co–P 850 was carried out by TEM (Fig. 3). The TEM images shown in Fig. 3a and b revealed the 3D microstructure of Co–P 850, in which nanoparticles of different sizes were well embedded in the carbon nanosheets. The crystalline spacing of the carbon nanosheets seen in Fig. 3b is approx. 0.33–0.35 nm, which is close to the thickness of the graphite layer (0.35 nm) (Chen et al., 2019). This suggests that the nanoparticles were tightly immobilized in graphite layers, which provided high stability. In addition, the TEM element mapping results (shown in Fig. 3c) confirmed that the granular nanoparticles observed in the TEM images were Co/Fe oxide nanoparticles formed in the carbonization process. Natural peat may contain a small amount of iron, and our previous work also specified the existence of iron in NaOH–P (Leiviskä et al., 2018). Therefore, one possible explanation is that the cobalt ions were adsorbed onto the same adsorption sites of NaOH–P as the iron ions. The atomic proportion of cobalt and iron measured in different catalyst particles varied considerably in the other TEM element mapping results shown in Fig. S2, with cobalt dominating in most cases. A possible explanation is that most of the adsorption sites on NaOH–P were saturated not with iron, but with some other ions instead. This means that these sites could then bind cobalt from the water until saturation was achieved. Therefore, cobalt and iron formed Co/Fe oxide nanoparticles in different proportions in the carbonization process.

The XPS survey spectrum and the Co2p, C1s and N1s high-resolution spectra of Co–P 850 are shown in Fig. 4. The main elements found in the XPS survey spectrum of Co–P 850 (Fig. 4a) were carbon, oxygen, nitrogen and cobalt. The atomic percentages of C, O, N and Co in Co–P 850 were 88.9%, 7.7%, 2.0% and 1.5% (Table S3), respectively. Additionally, a minor Fe2p peak was observed in the survey spectrum of all of the samples. The Co content increased with an increasing carbonization temperature and thus the atomic percentage of cobalt in Co–P 850 was the highest among the four carbonized samples. This phenomenon can be attributed to the higher weight loss of organic matter at the higher carbonization temperature, supported by the results of TGA analysis and the yield of the four catalysts. We deduced that a large amount of sp^2 carbon was present in Co–P 850. This was based on the sharp peak of C–C and the π-π * shake-up feature observed in the C1s spectrum (Fig. 4b), the graphite layer demonstrated in the TEM analysis and the characteristic diffraction peaks at 30.3° of graphite-3R (003) plane shown in the XRD pattern (Fig. S4). Therefore, we chose the C1s spectrum of 284.4 eV to carry out a charge shift for all of the XPS spectra (Leiro et al., 2003; Xie et al., 2017). The C1s spectrum showed two components (Fig. 4b) at 284.4 eV and 285.2 eV, which could be assigned to the C–C (sp^2 and sp^3 carbon) and C–O components in Co–P 850 (Du et al., 2020; Duan et al., 2019). The asymmetric tail towards the higher binding energy and the π-π * shake-up feature at 289.7 eV observed in the C1s further confirmed the results of the TEM and XRD analyses that a graphite layer was formed during the carbonization process (Leiro et al., 2003; Xie et al., 2017).

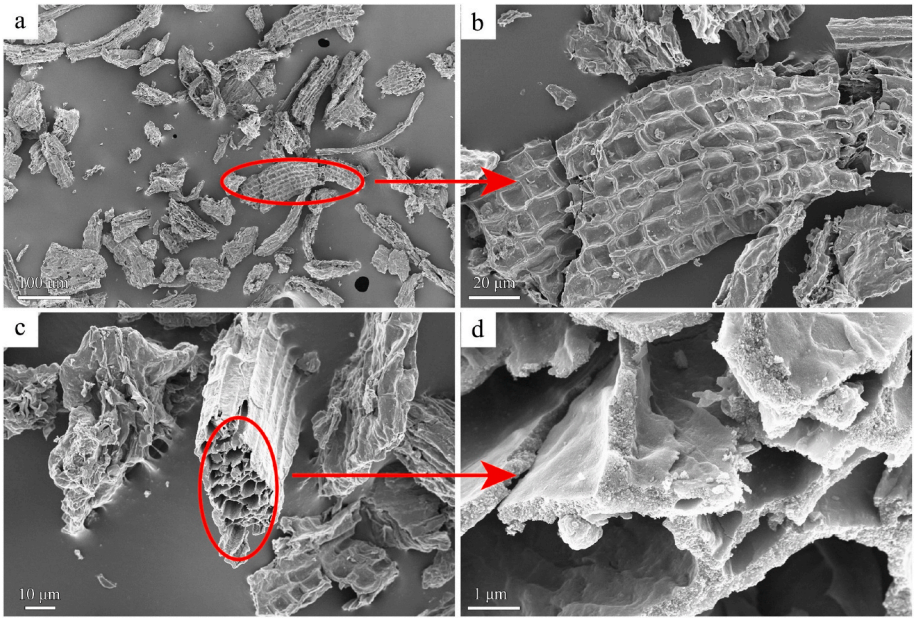

Fig. 2. FESEM images of Co–P 850. (a) Overall view (Mag × 360); (b) Uneven surface (Mag × 1700); (c) Porous structure (Mag × 2000); (d) Porous structure (Mag × 35,000).

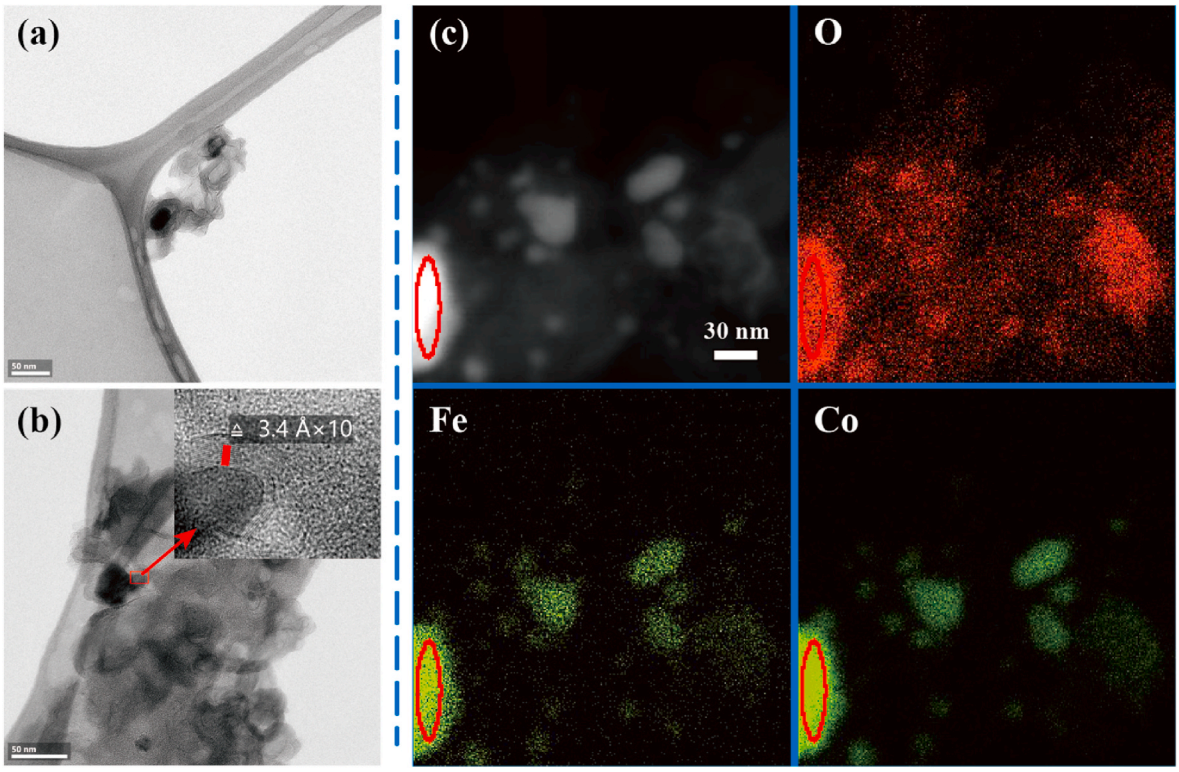

Fig. 3. (a) and (b) TEM images of Co–P 850; (c) TEM element mapping of Co–P 850.

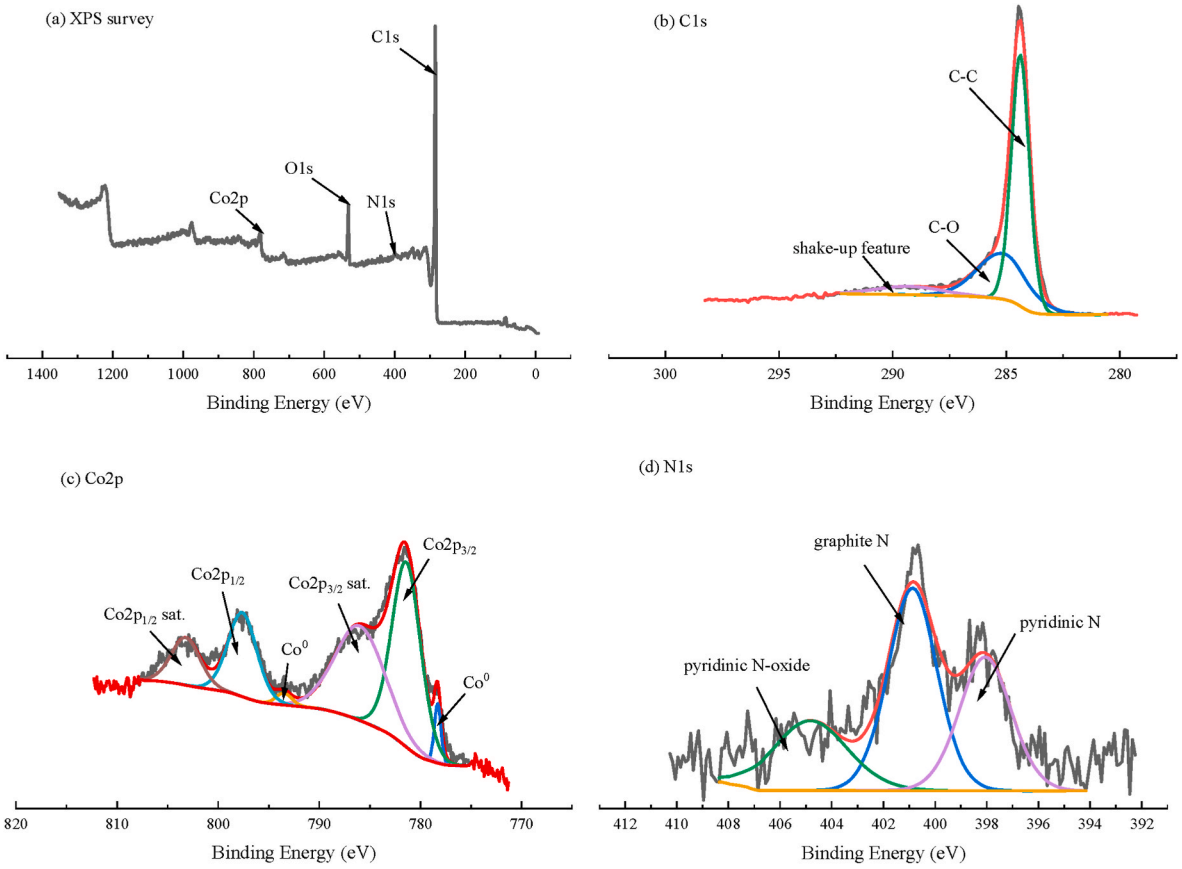

Fig. 4. (a) XPS survey spectrum of Co–P 850; (b) C1s, (c) Co2p and (d) N1s high-resolution XPS spectra of Co–P 850.

The Co2p XPS spectrum is shown in Fig. 4c. The main $Co2p_{1/2}$ and $Co2p_{3/2}$ peaks were observed at 797.6 and 781.5 eV, and could be related to cobalt(II) oxide (CoO). The binding energy separation between $Co2p_{3/2}$ and $Co2p_{1/2}$ was 16.1 eV, which allowed us to exclude the presence of Co^{3+} (Biesinger et al., 2011; Fantauzzi et al., 2019). Furthermore, the strong and wide satellite peaks at around 803.2 eV and 786.6 eV are consistent with the CoO spectrum reported in previous studies (Biesinger et al., 2011; Fantauzzi et al., 2019), indicating that the main Co species in Co–P 850 was probably CoO. The XRD pattern did not provide any further evidence as no cobalt oxide crystal structures were detected, probably due to the minimal amount and their nano-crystalline property. The $Co2p_{3/2}$ and $Co2p_{1/2}$ peaks of Co^0 were seen at 778.2 eV and 793.5 eV (Biesinger et al., 2011). In addition to Co–P 850, the Co^0 peaks were also observed in Co–P 700 and Co–P 800 (Figs. S3b and c). The XRD pattern of Co–P 850 also showed four main peaks at 51.5°, 60.5°, 90.4° and 113.0°, corresponding to the (111), (200), (220) and (311) planes of metallic Co. This implies that a small fraction of Co^{2+} was reduced to metallic Co during the carbonization process (Zhong et al., 2019). The N1s XPS spectrum (Fig. 4d) showed three components ascribed to pyridinic N (398.1 eV), graphite N (400.8 eV) (Chen et al., 2019; Du et al., 2020) and pyridinic N-oxide (404.8 eV) (Tian et al., 2018), which originated from natural peat.

3.2. Catalytic degradation of ibuprofen

The degradation performance of ibuprofen with different carbonized peat catalysts and PMS is shown in Fig. 5a. Compared to Co–P 600/PMS and Co–P 700/PMS, the ibuprofen degradation with Co–P 800/PMS was much more efficient, since 90% of the ibuprofen was decomposed within 120 min of the reaction at a degradation rate of 0.024 1/min. The Co–P 850/PMS system exhibited the highest degradation performance (k = 0.069 1/min) for IBU as no IBU at all was detected after 120 min of the reaction with Co leaching of 387 μg/L. The catalyst may have lost some catalytic activity as a result of Co leaching. Nevertheless, we found that the Co–P 850 was proven to be reusable (Fig. 5b). In addition, DOC measurements were carried out to evaluate the mineralization of the IBU and the catalytic efficiency of Co–P 850. The DOC was 6.23 mg/L and 3.82 mg/L after 1 h and 2 h reaction time, respectively (Fig. S5). This indicated that, although the IBU was not detected after 1 h, the mineralization of IBU and its degradation intermediates was occurring. After 5 h reaction time, the DOC of the solution was 2.01 mg/L and thus nearly 76.1% of DOC had been removed. Therefore, we recommend that some post-treatment such as adsorption or a biological process be applied to eliminate transformation products.

The Co-free carbonized peat (P-850) showed very poor catalytic properties, as only around 5% of the IBU was removed after 120 min. We can infer from the results that a higher carbonization temperature (800 °C–850 °C) and insertion of cobalt are essential for the synthesis of Co-doped catalyst from peat. One possible reason is that a stronger interaction between the carbon and Co/Fe oxide nanoparticles is formed at the higher carbonization temperature, which reduces the loss of cobalt after the prepared catalyst is washed with ethanol and deionized water. This is supported by the fact that Co–P 850 had the highest amount of Co on its surface according to the XPS analyses (see characteristics of the Co-loaded catalysts, section 3.1). The higher amount of cobalt provided more available catalytic sites for PMS activation and thus higher ibuprofen degradation efficiency. The catalytic sites of Co–P 850 were cobalt and cobalt oxides. The activation mechanism of PMS could be attributed to the heterogeneous catalysis provided by the embedded transition metal Co(II) in the carbon matrix, and the homogeneous catalysis resulting from the cobalt ions leached from the catalyst (Eq. S5) (Li et al., 2016).

The reusability test of Co–P 850 (Fig. 5b) without regeneration shows that, although degradation decreased after 120 min of reaction time, more than 90% and 80% of the ibuprofen was degraded in the second and third runs, respectively. On the other hand, thermal regeneration has been proven to be a feasible option to recover catalytic performance (Chen et al., 2019; Duan et al., 2019). Therefore, we selected the Co–P 850 catalyst for further studies.

The effects of catalyst dosage, PMS dosage, pH and temperature on IBU degradation with the Co–P 850/PMS system are displayed in Fig. 6. The ibuprofen degradation performance was improved as the catalyst dosage increased (Fig. 6a), whereas no degradation of IBU occurred without a catalyst. The IBU degradation rate increased from 0.021 to 0.071 1/min when the catalyst dosage was increased from 0.05 g/L to 0.2 g/L. However, the degradation efficiency improved only slightly when the catalyst dosage was higher than 0.1 g/L (rate constant for 0.069 to 0.071 1/min). This can be attributed to the adequate number of catalytic sites for PMS activation when the catalyst dosage reached 0.1 g/L, meaning that the available PMS (10 mM) was the limiting factor for the reaction at higher catalyst dosages (0.15 and 0.2 g/L). Similar results were observed for IBU degradation at a different PMS dosage (Fig. 6b). Only a limited enhancement of the rate constant was observed (from 0.062 to 0.074 1/min) when the PMS dosage was increased from 1 to 4 mM, implying that the available catalytic sites on Co–P 850 were gradually saturated with increasing PMS dosage. The IBU adsorption capacity of Co–P 850 was also tested without the addition of PMS. We found that only 13.8% of the ibuprofen was removed after 2 h of adsorption. As a result, we determined that suitable dosages of catalyst and PMS for IBU degradation were 0.1 g/L and 2 mM, respectively.

The effect of pH on ibuprofen degradation is shown in Fig. 6c. The IBU degradation performance was sensitive to pH change. Neutral (pH = 7.5) and slightly acidic conditions (pH = 5 and 6) were beneficial for degradation. However, degradation was inhibited at lower pH (pH =

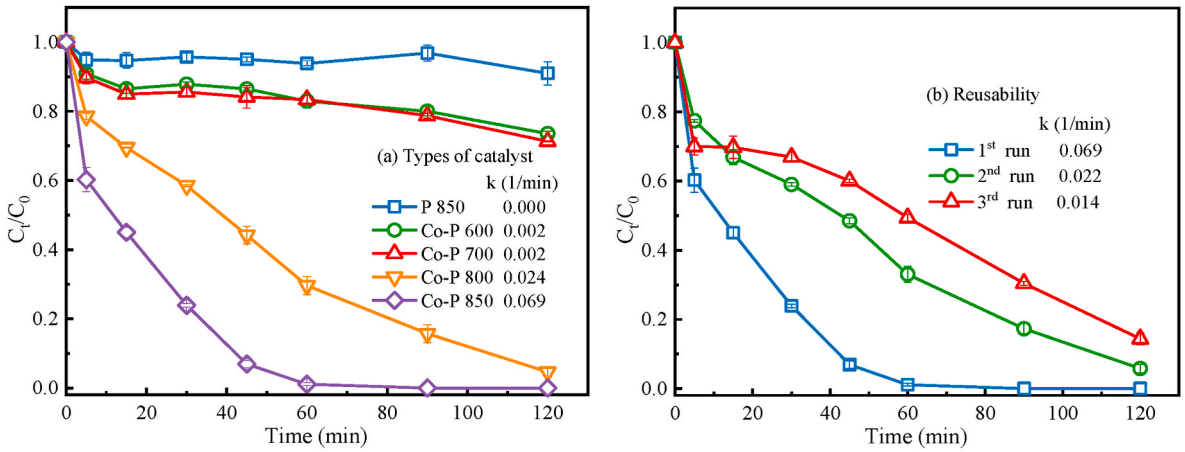

Fig. 5. (a) IBU degradation by different types of catalyst; (b) reusability of Co–P 850 ($[IBU]_0$ = 10 mg/L, $[PMS]_0$ = 2 mM, catalyst dosage = 0.1 g/L, pH = 7.5).

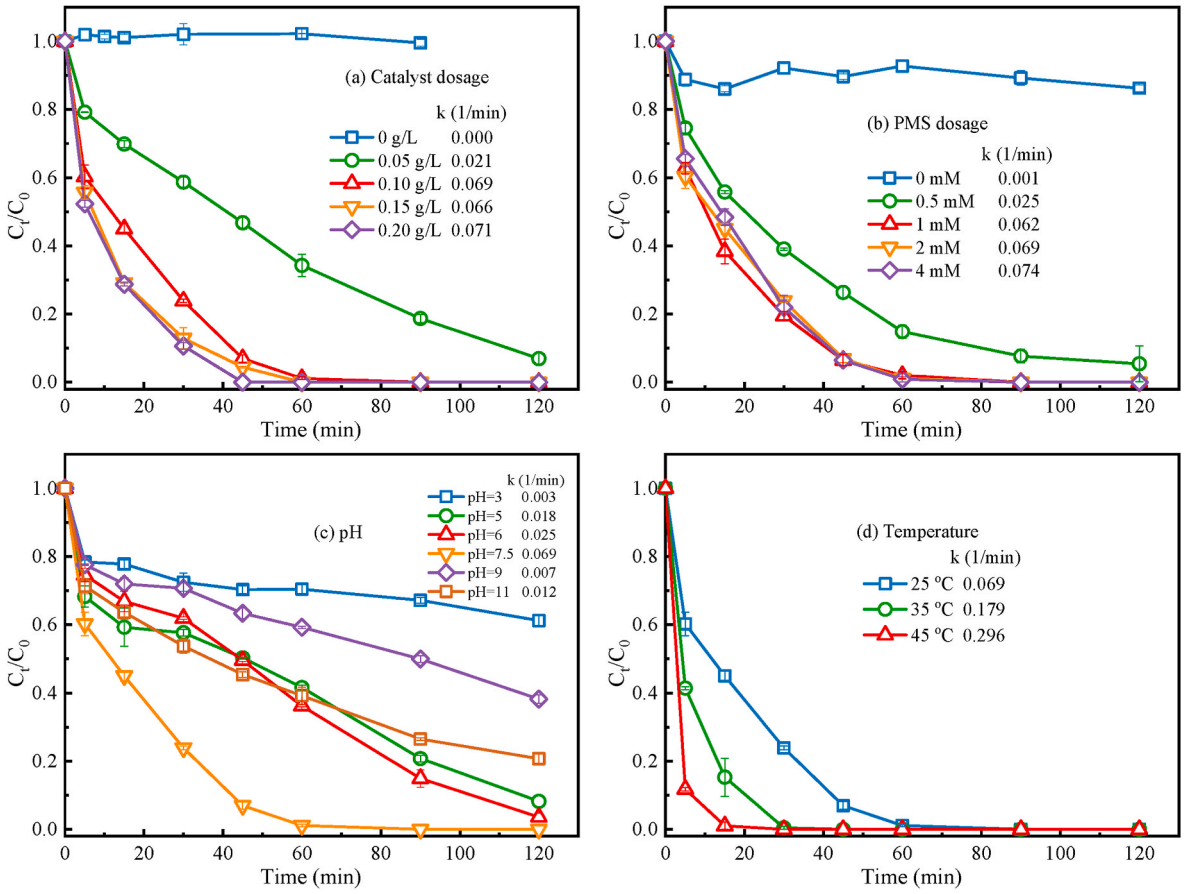

Fig. 6. Ibuprofen degradation with Co–P 850/PMS system under different conditions: (a) catalyst dosage; (b) PMS dosage; (c) pH; (d) catalytic temperature ($[IBU]_0$ = 10 mg/L, $[PMS]_0$ = 2 mM, Co–P 850 dosage = 0.1 g/L).

3), showing a dramatic decrease in the rate constant (0.003 1/min). In addition, alkaline conditions (pH = 9 and 11) had an adverse effect on the degradation (rate constant of 0.007 and 0.012 1/min, respectively). The low degradation at high pH could be attributed to the transformation of sulphate radical into hydroxyl radical, as described in Eq. (2), which consumed the sulphate radical and slowed down the degradation rate (Wang and Wang, 2018; Yang et al., 2010).

$$SO_4^{\cdot-} + H_2O \rightarrow SO_4^{2-} + \cdot OH + H^+ \quad (2)$$

It has been reported that high temperature is beneficial for sulphate radical generation; a high temperature (over 50 °C) could directly cause the fission of the O–O bond of PMS to generate the sulphate radical (Wang and Wang, 2018; Shi et al., 2012; Ghauch et al., 2012). As shown in Fig. 6d, the rate constant steadily increased to 0.069, 0.179 and 0.296 1/min when the temperature increased to 25 °C, 35 °C and 45 °C, respectively. Thus, ibuprofen degradation was greatly enhanced at higher temperature and complete degradation was achieved within 30 min below 45 °C.

3.3. Effect of co-existing anions on ibuprofen degradation

It has been reported that the degradation of organic pollutants by radical reaction is affected by co-existing ions (Duan et al., 2019; Hammouda et al., 2018). Therefore, a set of degradation experiments were performed with bicarbonate, phosphate, nitrate and chloride at different concentration levels (2, 5 and 10 mM) to investigate the effect of co-existing ions on ibuprofen degradation (pH = 7.5). As illustrated in Fig. 7a, the degradation performance was slightly improved in the presence of 2 mM bicarbonate, whereas higher concentrations of bicarbonate (5 mM and 10 mM) significantly inhibited IBU degradation: the rate constant dropped from 0.069 to 0.003 1/min compared to the control experiment (without added ions). Inhibition was mainly due to the scavenging of reactive radicals by HCO_3^- and CO_3^{2-} (Eqs. (3)–(6)), which has been proven previously (Du et al., 2020; Hammouda et al., 2018).

In contrast to bicarbonate, the degradation of ibuprofen was inhibited only slightly in the presence of phosphate. The rate constants were 0.057, 0.036 and 0.045 1/min at phosphate concentrations of 2, 5 and 10 mM, respectively. This was mainly due to the generation of $H_2PO_4^-$ from the hydrolysis of PO_4^{3-}, which is known as a scavenger for ·OH that inhibits IBU degradation by the ·OH pathway (Duan et al., 2019). In addition, the hydrolysis of phosphate also reduced the concentration of H^+, which led to an increase in the solution pH. This may have affected the degradation performance. Similarly, the addition of nitrate at different levels (2, 5 and 10 mM) showed a very weak inhibitory effect on IBU degradation, as complete degradation could still be achieved with rate constants of 0.029–0.039 1/min after 2 h of reaction time (Fig. 7c). This has been explained by the slow reaction of nitrate with sulphate radicals via Eq. (7), and the generation of nitrate radical that slightly suppressed the degradation efficiency (Exner et al., 1992; Tan et al., 2013).

A clear inhibitory effect on IBU degradation was observed with the addition of chloride (Fig. 7d). The rate constant was as low as 0.003 1/min. Only about 30–35% of the ibuprofen was removed after 2 h of reaction time when we varied the chloride concentration between 2 and 10 mM. It has been frequently reported that chlorine radicals with a lower redox potential, such as ·Cl, $\cdot Cl_2^-$ and $\cdot ClOH^-$, are generated via Eqs. (8)–(10) (Deng et al., 2017; Du et al., 2020; C. Li et al., 2019a), and that these chlorine radicals are not active enough for ibuprofen degradation. Therefore, the generation of secondary chlorine radicals from

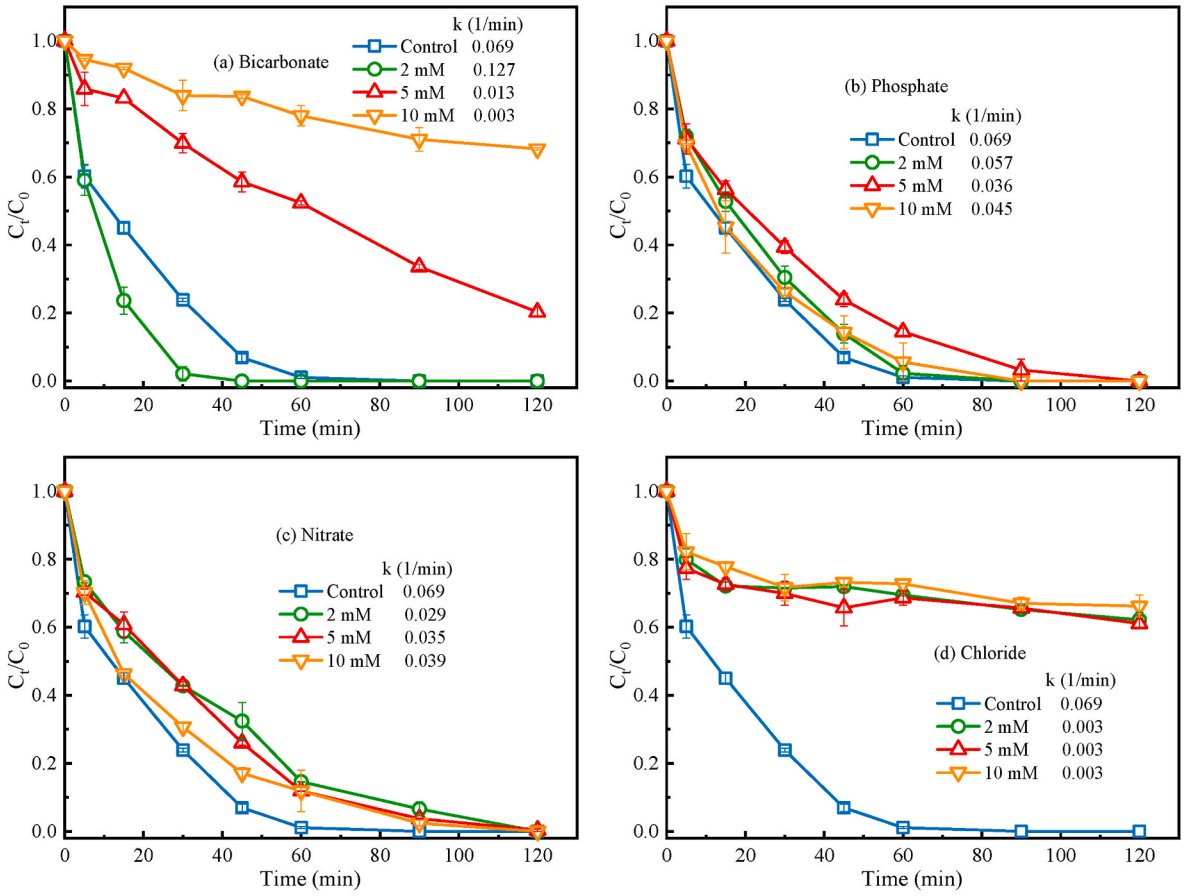

Fig. 7. Effect of inorganic anions on the degradation of ibuprofen: (a) bicarbonate; (b) phosphate; (c) nitrate; (d) chloride ($[IBU]_0$ = 10 mg/L, $[PMS]_0$ = 2 mM, Co–P 850 dosage = 0.1 g/L, pH = 7.5).

reactive sulphate radical species might be the reason why the degradation process was hindered.

$$CO_3^{2-} + SO_4^{\cdot-} \rightarrow CO_3^{\cdot-} + SO_4^{2-} \quad (3)$$

$$HCO_3^- + SO_4^{\cdot-} \rightarrow HCO_3\cdot + SO_4^{2-} \quad (4)$$

$$CO_3^{2-} + \cdot OH \rightarrow CO_3^{\cdot-} + OH^- \quad (5)$$

$$HCO_3^- + \cdot OH \rightarrow CO_3^{\cdot-} + H_2O \quad (6)$$

$$SO_4^{\cdot-} + NO_3^- \rightarrow SO_4^{2-} + \cdot NO_3 \quad (7)$$

$$Cl^- + SO_4^{\cdot-} \rightarrow Cl\cdot + SO_4^{2-} \quad (8)$$

$$Cl^- + Cl\cdot \rightarrow Cl_2^{\cdot-} \quad (9)$$

$$Cl_2^{\cdot-} + H_2O \rightarrow ClOH^{\cdot-} + H^+ + Cl^- \quad (10)$$

3.4. Identification of radical species

It has been reported that various types of radicals, such as hydroxyl, sulphate, sulphite, peroxysulphate and peroxymonosulphate anion, are generated in the PMS activation process (Hammouda et al., 2018; C. Li et al., 2019a). Among them, the dominant reactive radicals that contribute to the degradation of organic pollutants are ·OH and $SO_4^{\cdot-}$, due to their high oxidation potential. However, other radical and non-radical pathways, such as the superoxide anion radical ($O_2^{\cdot-}$) and singlet oxygen ($^1O_2$), have also been shown to provide a non-negligible effect on degradation. Therefore, it is important to identify the radical species and determine the most effective radical in the Co–P 850/PMS system. We identified the generation of radicals by a direct method using electron paramagnetic resonance (EPR), and indirect methods using radical scavengers (p-BQ, L-his, EtOH and TBA).

p-BQ is usually used as a scavenging reagent for $O_2^{\cdot-}$ ($k = 1.0 \times 10^9$/M·s). As shown in Fig. 8a, the degradation of ibuprofen was inhibited by an increasing amount of p-BQ. Only 50–56% of the IBU was removed after 120 min of reaction time when p-BQ was present (5–20 mM). This indicated that the generation of $O_2^{\cdot-}$ is a fairly important pathway for IBU degradation. L-histidine, on the other hand, has been used in many studies as a unique scavenger for $^1O_2$ (Chen et al., 2019; Sun et al., 2019). As shown in Fig. 8b, only around 8% of the IBU was removed with a rate constant of 0.0005 1/min in the presence of 5 mM of L-his. However, it does not seem reasonable that the $^1O_2$ would contribute more than 90% of the IBU degradation. It has been reported that the addition of L-his leads to fast consumption of PMS and results in poor degradation performance (Yang et al., 2018). Therefore, EPR needs to be employed further to investigate the generation and effect of $^1O_2$. The 8% removal of IBU could be attributed to adsorption by Co–P 850, which is consistent with the adsorption test presented in section 3.2 (Fig. 6b). EtOH is an effective scavenger for both $SO_4^{\cdot-}$($k = 1.6–7.7 \times 10^8$/M·s). and ·OH ($k = 1.2–2.8 \times 10^8$/M·s) radicals. In the presence of EtOH (Fig. 8c), the IBU degradation efficiency decreased significantly. The degradation efficiencies ranged between 30 and 32% in the presence of EtOH (100–500 mM) after 120 min of reaction time. This result suggests that both $SO_4^{\cdot-}$ and ·OH contribute significantly to IBU removal. TBA is a typical scavenging agent for ·OH ($k = 3.8–7.6 \times 10^8$/M·s). The influence of TBA on IBU degradation is shown in Fig. 8d. The degradation of IBU was slightly affected by 100 mM of TBA since as much as 83% of the IBU was removed with a rate constant of 0.0183 1/min. A higher

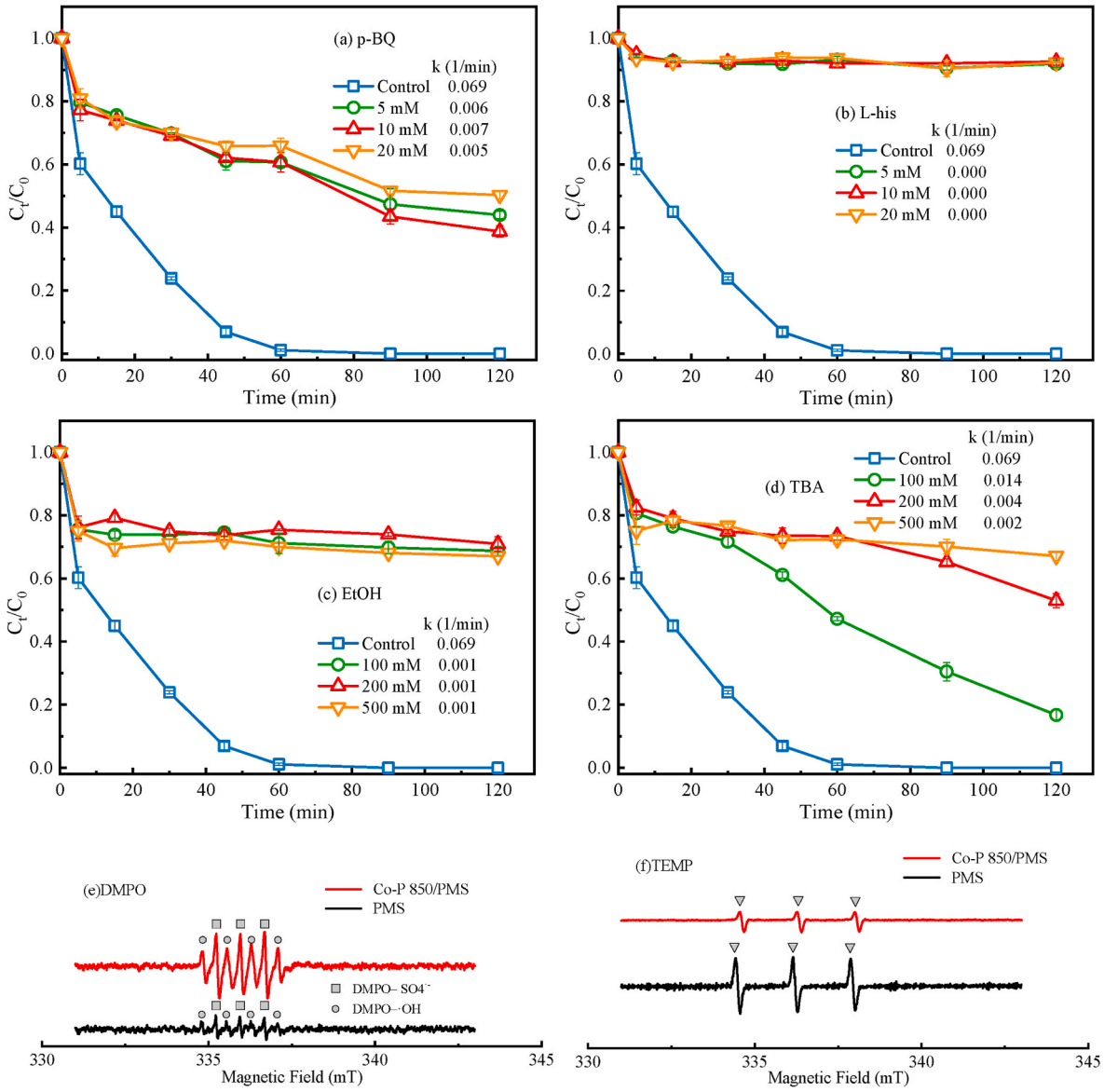

Fig. 8. Degradation of IBU with Co–P 850 in the presence of multiple quenching reagents: (a) p-BQ; (b) L-his; (c) EtOH; (d) TBA ($[IBU]_0 = 10$ mg/L, $[PMS]_0 = 2$ mM, Co–P 850 dosage = 0.1 g/L); EPR test with (e) DMPO and (f) TEMP.

inhibitory effect on IBU degradation, i.e. 33% IBU removal with a rate constant of 0.0021 1/min, was observed when the concentration of TBA was increased to 500 mM. This implies that the radical pathway involving ·OH is also important for IBU degradation. To sum up, these results confirmed that the $SO_4^{\cdot-}$, ·OH and $O_2^{\cdot-}$ pathways play indispensable roles in the degradation of ibuprofen in the Co–P 850/PMS system.

Further EPR analysis was conducted to investigate the evolution of non-radicals and radicals in the Co–P 850 system. DMPO is effective for trapping $SO_4^{\cdot-}$ and ·OH, and TEMP is known as a trapping reagent for $^1O_2$. As shown in Fig. 8e, weak signals of DMPO-·OH and DMPO– $SO_4^{\cdot-}$ were observed in the sole PMS system (Kang et al., 2018). When Co–P 850 was added, the signals of DMPO-·OH and DMPO– $SO_4^{\cdot-}$ were improved significantly, which suggests a mass generation of $SO_4^{\cdot-}$ and ·OH radicals in the Co–P850/PMS system. Fig. 8f shows that the characteristic three-line EPR spectrum signal of $^1O_2$ was observed both in the sole PMS and the Co–P850/PMS systems. However, the signal intensity of $^1O_2$ was reduced when Co–P 850 was added. As presented in section 3.2 on the catalytic degradation of ibuprofen (Fig. 6a), the results of the degradation experiments showed that the absence of Co–P 850 led to very poor IBU degradation performance. This suggests that $^1O_2$ was not the main radical that contributed to IBU degradation. Therefore, the generation of $SO_4^{\cdot-}$ and ·OH radicals was strongly promoted in the Co–P850/PMS system and both of them contributed to the high IBU degradation efficiency.

3.5. Degradation pathway analysis

The degradation intermediates of IBU were detected by HPLC ion-trap mass spectrometry (MS). The MS spectra of the IBU solution, IBU degradation after 1 min and IBU degradation after 5 min are shown in Fig. S6. The 13 intermediate degradation compounds (P1 to P13) of IBU were analysed according to the MS spectra and based on the literature data. They are shown in Fig. 9a (Illés et al., 2013; Jin et al., 2018; Li et al., 2014; Madhavan et al., 2010; Zhang et al., 2019). The ibuprofen structure and predicted reaction sites of the IBU molecule by density functional theory (DFT) calculations (the highest occupied molecular orbital (FED_{HOMO}) and the lowest unoccupied molecular orbital (FED_{LUMO})) are shown in Fig. 9b and c. The first step of IBU degradation mainly involved the introduction of hydroxyl groups (–OH) into the isobutyl group, propionic acid or benzene ring via either $SO_4^{\cdot-}$ or ·OH,

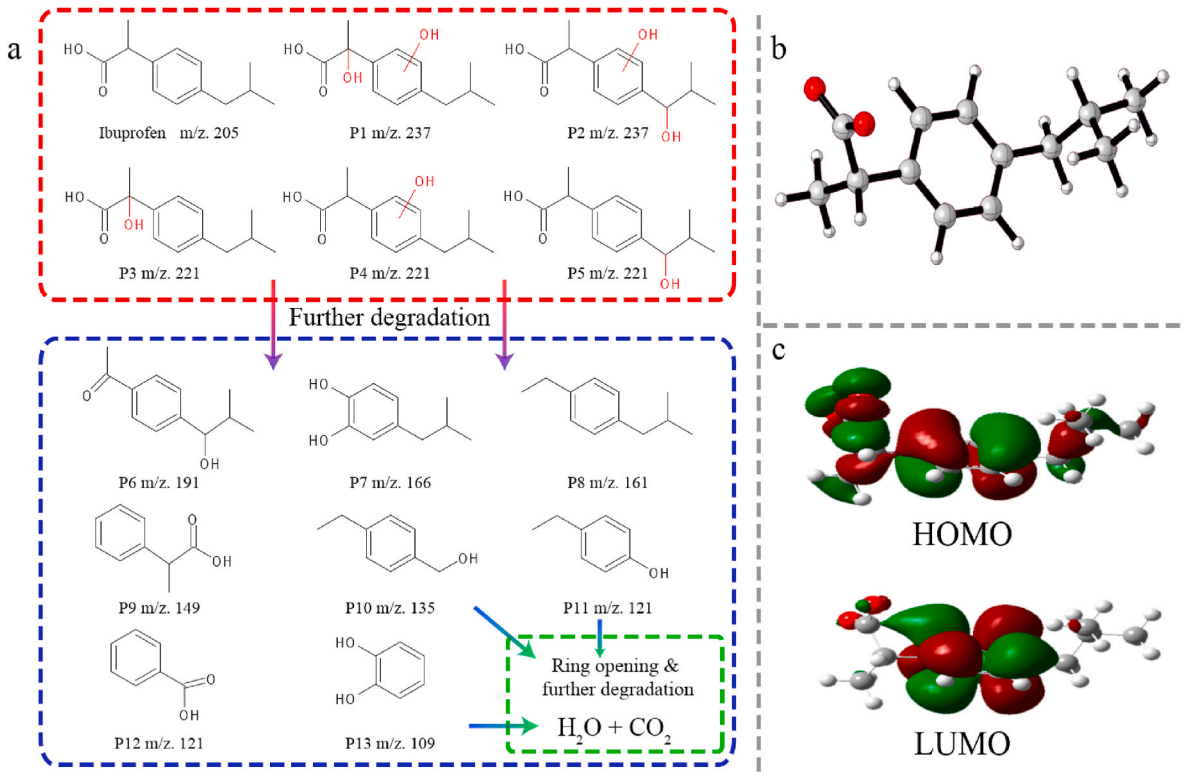

Fig. 9. (a) Possible degradation pathways and degradation intermediates of ibuprofen in the Co–P 850/PMS system; (b) chemical structure of IBU; (c) FED_{HOMO} and FED_{LUMO} of the IBU molecule.

generating either P1, P2 (m/z: 237) or P3, P4 and P5 (m/z: 221) (Fig. 9a) (Li et al., 2014; Méndez-Arriaga et al., 2010; Xiang et al., 2016). This result was in agreement with the DFT calculations, which revealed that the high electron density parts of the IBU molecule were located at the benzene ring, the secondary carbon atom of the carboxyl group and the isobutyl group. These are easily attacked by radicals. Then, the generated P1 to P5 were further degraded by the decarboxylation, hydroxylation and demethylation processes that produce P6 to P13 (Li et al., 2014; Wang et al., 2016; Xiang et al., 2016). Finally, a ring cleavage process occurred and further mineralization to CO_2 and H_2O was achieved.

4. Significance of the study

Over the decades, biomaterials such as reed, sawdust, peanut husks and peat have been considered to be ideal materials for preparing biosorbents to adsorb metals from water (Leiviskä et al., 2018; Mungondori et al., 2017; Southichak et al., 2006). Although most of the biosorbents can be regenerated and used several times, the problem of final disposal cannot be avoided (Huang et al., 2020; Swarnalatha and Ayoob, 2016). The conventional disposal methods for spent sorbents are landfill and incineration (Ramrakhiani et al., 2017). Ever-increasing landfill taxes and more stringent restrictions make landfilling an undesirable choice (Huang et al., 2020; Vijayaraghavan and Yun, 2008). Moreover, the incineration of biosorbents is receiving more and more criticism due to the generation of hazardous volatiles and metal-enriched ash (Vijayaraghavan and Yun, 2008). Recently, a novel research proposed a safe disposal method that seals the spent biosorbent in glass to avoid secondary pollution (Ramrakhiani et al., 2017). One drawback of this process is the high consumption of energy, which may limit its application. Some transition metals, such as Co, Cu, Ni and Mn, are valuable metals that can be used as active components for environmental catalysis such as advanced oxidation processes (AOPs) to eliminate organic contamination (Ghanbari and Moradi, 2017; Oh et al., 2016; Wang and Wang, 2018). Is it possible to convert a metal-loaded biosorbent into a catalyst to achieve the full recycling of the spent biosorbent?

This study showed that an efficient catalyst for drug degradation could be produced from waste material. NaOH–P is a promising biosorbent which has a high metal adsorption capacity. Once used in the treatment of metal-rich effluent, it can be turned into a new valuable product. The peat-derived catalyst, Co–P 850, was proven to have good PMS activation performance and high IBU degradation efficiency. This new circular economy solution can solve the disposal problem of spent biosorbent and allows the full recycling of the carbon matrix and its active metal components in a sustainable way.

5. Conclusions

We successfully prepared a Co-doped, carbon-based catalyst by the carbonization method using cobalt-saturated peat as a precursor. TEM and XPS analyses indicated that Co/Fe oxide nanoparticles were formed and immobilized in the carbon matrix in Co–P 850, providing good catalytic performance and stability. The Co–P 850/PMS system exhibited the best ibuprofen degradation performance: 10 mg/L ibuprofen was fully removed within 60 min. The favourable pH range for ibuprofen degradation in the Co–P 850/PMS system was from 5 to 7.5. Co-existing ions such as bicarbonate and chloride limited the ibuprofen degradation performance significantly, whereas phosphate and nitrate had only a minor effect. The results of quenching experiments and the electron paramagnetic resonance test implied that $SO_4^{\cdot-}$, ·OH and $O_2^{\cdot-}$ radicals contributed to the efficient degradation of ibuprofen. We also analysed the degradation intermediates in the ibuprofen degradation process and a possible degradation pathway using mass spectrometry spectra and density functional theory calculations. These results indicate that the major degradation mechanisms of ibuprofen are hydroxylation, decarboxylation and demethylation. As the disposal of spent sorbent is a challenge, this study provides a potential option for reusing spent sorbents as catalysts for the degradation of ibuprofen and other organic

pollutants.

CRediT author statement

Zhongfei Ren: Conceptualization, Methodology, Data curation, Writing – original draft, Writing- Reviewing and Editing, Software, Formal analysis, Visualization, Investigation, Validation. Henrik Romar and Toni Varila: Resources, Reviewing and Editing, Carbonization of the materials. Xing Xu: Conceptualization, Resources, Reviewing and edition, Formal analysis, quantum computing. Zhao Wang and Mika Sillanpää;: Resources, Reviewing and editing, EPR test. Tiina Leiviskä: Supervision, Funding acquisition, Conceptualization, Methodology, Resources, Writing- Reviewing and Editing.

Declaration of competing interest

The authors declare that they have no known competing financial interests or personal relationships that could have appeared to influence the work reported in this paper.

Acknowledgements

The research was supported by the Finnish National Agency for Education through the EDUFI Fellowship (TM-18-10999).

Appendix A. Supplementary data

Supplementary data to this article can be found online at https://doi.org/10.1016/j.envres.2020.110564.

References

Abbasoglu, R., 2006. Ab initio and DFT study on the electrophilic addition reaction of bromine to tetracyclo[5.3.0.02,6.03,10]deca–4,8–diene. J. Mol. Model. 12, 991–995. https://doi.org/10.1007/s00894-006-0113-3.

Anipsitakis, G.P., Dionysiou, D.D., Gonzalez, M.A., 2006. Cobalt-Mediated activation of peroxymonosulfate and sulfate radical attack on phenolic compounds. Implications of chloride ions. Environ. Sci. Technol. 40, 1000–1007. https://doi.org/10.1021/es050634b.

Archer, E., Petrie, B., Kasprzyk-Hordern, B., Wolfaardt, G.M., 2017. The fate of pharmaceuticals and personal care products (PPCPs), endocrine disrupting contaminants (EDCs), metabolites and illicit drugs in a WWTW and environmental waters. Chemosphere 174, 437–446. https://doi.org/10.1016/j.chemosphere.2017.01.101.

Biesinger, M.C., Payne, B.P., Grosvenor, A.P., Lau, L.W.M., Gerson, A.R., Smart, R.StC., 2011. Resolving surface chemical states in XPS analysis of first row transition metals, oxides and hydroxides: Cr, Mn, Fe, Co and Ni. Appl. Surf. Sci. 257, 2717–2730. https://doi.org/10.1016/j.apsusc.2010.10.051.

Chen, C., Ma, T., Shang, Y., Gao, B., Jin, B., Dan, H., Li, Q., Yue, Q., Li, Y., Wang, Y., Xu, X., 2019. In-situ pyrolysis of Enteromorpha as carbocatalyst for catalytic removal of organic contaminants: considering the intrinsic N/Fe in Enteromorpha and non-radical reaction. Appl. Catal. B Environ. 250, 382–395. https://doi.org/10.1016/j.apcatb.2019.03.048.

Chen, L., Cai, T., Sun, W., Zuo, X., Ding, D., 2017. Mesoporous bouquet-like Co3O4 nanostructure for the effective heterogeneous activation of peroxymonosulfate. J. Taiwan Inst. Chem. Eng. 80, 720–727. https://doi.org/10.1016/j.jtice.2017.09.007.

Chiou, C.T., Kile, D.E., Rutherford, D.W., Sheng, G., Boyd, S.A., 2000. Sorption of selected organic compounds from water to a peat soil and its humic-acid and humin Fractions: potential sources of the sorption nonlinearity. Environ. Sci. Technol. 34, 1254–1258. https://doi.org/10.1021/es990261c.

Deblonde, T., Cossu-Leguille, C., Hartemann, P., 2011. Emerging pollutants in wastewater: a review of the literature. Int. J. Hyg Environ. Health 214, 442–448. https://doi.org/10.1016/j.ijheh.2011.08.002.

Deng, J., Cheng, Y., Lu, Y., Crittenden, J.C., Zhou, S., Gao, N., Li, J., 2017. Mesoporous manganese Cobaltite nanocages as effective and reusable heterogeneous peroxymonosulfate activators for Carbamazepine degradation. Chem. Eng. J. 330, 505–517. https://doi.org/10.1016/j.cej.2017.07.149.

Du, W., Zhang, Q., Shang, Y., Wang, W., Li, Q., Yue, Q., Gao, B., Xu, X., 2020. Sulfate saturated biosorbent-derived Co-S@NC nanoarchitecture as an efficient catalyst for peroxymonosulfate activation. Appl. Catal. B Environ. 262, 118302. https://doi.org/10.1016/j.apcatb.2019.118302.

Duan, P., Ma, T., Yue, Y., Li, Y., Zhang, X., Shang, Y., Gao, B., Zhang, Q., Yue, Q., Xu, X., 2019. Fe/Mn nanoparticles encapsulated in nitrogen-doped carbon nanotubes as a peroxymonosulfate activator for acetamiprid degradation. Environ. Sci. Nano 6, 1799–1811. https://doi.org/10.1039/C9EN00220K.

Duan, P., Qi, Y., Feng, S., Peng, X., Wang, W., Yue, Y., Shang, Y., Li, Y., Gao, B., Xu, X., 2020. Enhanced degradation of clothianidin in peroxymonosulfate/catalyst system via core-shell FeMn @ N-C and phosphate surrounding. Appl. Catal. B Environ. 267, 118717. https://doi.org/10.1016/j.apcatb.2020.118717.

Exner, M., Herrmann, H., Zellner, R., 1992. Laser-based studies of reactions of the nitrate radical in aqueous solution. Berichte Bunsenges. Für Phys. Chem. 96, 470–477. https://doi.org/10.1002/bbpc.19920960347.

Fantauzzi, M., Secci, F., Angotzi, M.S., Passiu, C., Cannas, C., Rossi, A., 2019. Nanostructured spinel cobalt ferrites: Fe and Co chemical state, cation distribution and size effects by X-ray photoelectron spectroscopy. RSC Adv. 9, 19171–19179. https://doi.org/10.1039/C9RA03488A.

Ghanbari, F., Moradi, M., 2017. Application of peroxymonosulfate and its activation methods for degradation of environmental organic pollutants: Review. Chem. Eng. J. 310, 41–62. https://doi.org/10.1016/j.cej.2016.10.064.

Ghauch, A., Tuqan, A.M., Kibbi, N., 2012. Ibuprofen removal by heated persulfate in aqueous solution: a kinetics study. Chem. Eng. J. 197, 483–492. https://doi.org/10.1016/j.cej.2012.05.051.

Gogoi, H., Leiviskä, T., Heiderscheidt, E., Postila, H., Tanskanen, J., 2018. Removal of metals from industrial wastewater and urban runoff by mineral and bio-based sorbents. J. Environ. Manag. 209, 316–327. https://doi.org/10.1016/j.jenvman.2017.12.019.

Gu, Y., Yperman, J., Carleer, R., D'Haen, J., Maggen, J., Vanderheyden, S., Vanreppelen, K., Garcia, R.M., 2019. Adsorption and photocatalytic removal of Ibuprofen by activated carbon impregnated with TiO2 by UV–Vis monitoring. Chemosphere 217, 724–731. https://doi.org/10.1016/j.chemosphere.2018.11.068.

Gumbi, B.P., Moodley, B., Birungi, G., Ndungu, P.G., 2017. Detection and quantification of acidic drug residues in South African surface water using gas chromatography-mass spectrometry. Chemosphere 168, 1042–1050. https://doi.org/10.1016/j.chemosphere.2016.10.105.

Hammouda, S.B., Zhao, F., Safaei, Z., Ramasamy, D.L., Doshi, B., Sillanpää, M., 2018. Sulfate radical-mediated degradation and mineralization of bisphenol F in neutral medium by the novel magnetic Sr2CoFeO6 double perovskite oxide catalyzed peroxymonosulfate: influence of co-existing chemicals and UV irradiation. Appl. Catal. B Environ. 233, 99–111. https://doi.org/10.1016/j.apcatb.2018.03.088.

Hasan, Z., Khan, N.A., Jhung, S.H., 2016. Adsorptive removal of diclofenac sodium from water with Zr-based metal–organic frameworks. Chem. Eng. J. 284, 1406–1413. https://doi.org/10.1016/j.cej.2015.08.087.

Ho, Y.S., McKay, G., 2000. The kinetics of sorption of divalent metal ions onto sphagnum moss peat. Water Res. 34, 735–742. https://doi.org/10.1016/S0043-1354(99)00232-8.

Huang, D., Li, B., Ou, J., Xue, W., Li, J., Li, Z., Li, T., Chen, S., Deng, R., Guo, X., 2020. Megamerger of biosorbents and catalytic technologies for the removal of heavy metals from wastewater: preparation, final disposal, mechanism and influencing factors. J. Environ. Manag. 261, 109879. https://doi.org/10.1016/j.jenvman.2019.109879.

Ikhlaq, A., Brown, D.R., Kasprzyk-Hordern, B., 2014. Catalytic ozonation for the removal of organic contaminants in water on ZSM-5 zeolites. Appl. Catal. B Environ. 154–155, 110–122. https://doi.org/10.1016/j.apcatb.2014.02.010.

Illés, E., Takács, E., Dombi, A., Gajda-Schrantz, K., Rácz, G., Gonter, K., Wojnárovits, L., 2013. Hydroxyl radical induced degradation of ibuprofen. Sci. Total Environ. 447, 286–292. https://doi.org/10.1016/j.scitotenv.2013.01.007.

Jin, Y., Sun, S.-P., Yang, X., Chen, X.D., 2018. Degradation of ibuprofen in water by FeII-NTA complex-activated persulfate with hydroxylamine at neutral pH. Chem. Eng. J. 337, 152–160. https://doi.org/10.1016/j.cej.2017.12.094.

Kang, J., Duan, X., Wang, C., Sun, H., Tan, X., Tade, M.O., Wang, S., 2018. Nitrogen-doped bamboo-like carbon nanotubes with Ni encapsulation for persulfate activation to remove emerging contaminants with excellent catalytic stability. Chem. Eng. J. 332, 398–408. https://doi.org/10.1016/j.cej.2017.09.102.

Leiro, J.A., Heinonen, M.H., Laiho, T., Batirev, I.G., 2003. Core-level XPS spectra of fullerene, highly oriented pyrolitic graphite, and glassy carbon. J. Electron. Spectrosc. Relat. Phenom. 128, 205–213. https://doi.org/10.1016/S0368-2048(02)00284-0.

Leiviskä, T., Khalid, M.K., Gogoi, H., Tanskanen, J., 2018. Enhancing peat metal sorption and settling characteristics. Ecotoxicol. Environ. Saf. 148, 346–351. https://doi.org/10.1016/j.ecoenv.2017.10.053.

Li, C., Huang, Y., Dong, X., Sun, Z., Duan, X., Ren, B., Zheng, S., Dionysiou, D.D., 2019a. Highly efficient activation of peroxymonosulfate by natural negatively-charged kaolinite with abundant hydroxyl groups for the degradation of atrazine. Appl. Catal. B Environ. 247, 10–23. https://doi.org/10.1016/j.apcatb.2019.01.079.

Li, H., Wan, J., Ma, Y., Wang, Y., Chen, X., Guan, Z., 2016. Degradation of refractory dibutyl phthalate by peroxymonosulfate activated with novel catalysts cobalt metal-organic frameworks: mechanism, performance, and stability. J. Hazard Mater. 318, 154–163. https://doi.org/10.1016/j.jhazmat.2016.06.058.

Li, X., Wang, Y., Yuan, S., Li, Z., Wang, B., Huang, J., Deng, S., Yu, G., 2014. Degradation of the anti-inflammatory drug ibuprofen by electro-peroxone process. Water Res. 63, 81–93. https://doi.org/10.1016/j.watres.2014.06.009.

Li, Z., Gómez-Avilés, A., Sellaoui, L., Bedia, J., Bonilla-Petriciolet, A., Belver, C., 2019b. Adsorption of ibuprofen on organo-sepiolite and on zeolite/sepiolite heterostructure: synthesis, characterization and statistical physics modeling. Chem. Eng. J. 371, 868–875. https://doi.org/10.1016/j.cej.2019.04.138.

Madhavan, J., Grieser, F., Ashokkumar, M., 2010. Combined advanced oxidation processes for the synergistic degradation of ibuprofen in aqueous environments. J. Hazard Mater. 178, 202–208. https://doi.org/10.1016/j.jhazmat.2010.01.064.

Mailler, R., Gasperi, J., Coquet, Y., Deshayes, S., Zedek, S., Cren-Olivé, C., Cartiser, N., Eudes, V., Bressy, A., Caupos, E., Moilleron, R., Chebbo, G., Rocher, V., 2015. Study of a large scale powdered activated carbon pilot: removals of a wide range of

emerging and priority micropollutants from wastewater treatment plant effluents. Water Res. 72, 315–330. https://doi.org/10.1016/j.watres.2014.10.047.
Meierjohann, A., Brozinski, J.-M., Kronberg, L., 2016. Seasonal variation of pharmaceutical concentrations in a river/lake system in Eastern Finland. Environ. Sci. Process. Impacts 18, 342–349. https://doi.org/10.1039/C5EM00505A.
Méndez-Arriaga, F., Esplugas, S., Giménez, J., 2010. Degradation of the emerging contaminant ibuprofen in water by photo-Fenton. Water Res. 44, 589–595. https://doi.org/10.1016/j.watres.2009.07.009.
Mungondori, H.H., Mtetwa, S., Tichagwa, L., Katwire, D.M., Nyamukamba, P., 2017. Synthesis and application of a ternary composite of clay, saw-dust and peanut husks in heavy metal adsorption. Water Sci. Technol. 75, 2443–2453. https://doi.org/10.2166/wst.2017.123.
Oh, W.-D., Dong, Z., Lim, T.-T., 2016. Generation of sulfate radical through heterogeneous catalysis for organic contaminants removal: current development, challenges and prospects. Appl. Catal. B Environ. 194, 169–201. https://doi.org/10.1016/j.apcatb.2016.04.003.
Paíga, P., Santos, L.H.M.L.M., Ramos, S., Jorge, S., Silva, J.G., Delerue-Matos, C., 2016. Presence of pharmaceuticals in the Lis river (Portugal): sources, fate and seasonal variation. Sci. Total Environ. 573, 164–177. https://doi.org/10.1016/j.scitotenv.2016.08.089.
Peng, L., Shang, Y., Gao, B., Xu, X., 2021. Co3O4 anchored in N, S heteroatom co-doped porous carbons for degradation of organic contaminant: role of pyridinic N-Co binding and high tolerance of chloride. Appl. Catal. B Environ. 282, 119484. https://doi.org/10.1016/j.apcatb.2020.119484.
Ramrakhiani, L., Halder, A., Majumder, A., Mandal, A.K., Majumdar, S., Ghosh, S., 2017. Industrial waste derived biosorbent for toxic metal remediation: mechanism studies and spent biosorbent management. Chem. Eng. J. 308, 1048–1064. https://doi.org/10.1016/j.cej.2016.09.145.
Rastogi, A., Al-Abed, S.R., Dionysiou, D.D., 2009. Sulfate radical-based ferrous–peroxymonosulfate oxidative system for PCBs degradation in aqueous and sediment systems. Appl. Catal. B Environ. 85, 171–179. https://doi.org/10.1016/j.apcatb.2008.07.010.
Robles-Molina, J., Gilbert-López, B., García-Reyes, J.F., Molina-Díaz, A., 2014. Monitoring of selected priority and emerging contaminants in the Guadalquivir River and other related surface waters in the province of Jaén, South East Spain. Sci. Total Environ. 479–480, 247–257. https://doi.org/10.1016/j.scitotenv.2014.01.121.
Saeid, S., Tolvanen, P., Kumar, N., Eränen, K., Peltonen, J., Peurla, M., Mikkola, J.-P., Franz, A., Salmi, T., 2018. Advanced oxidation process for the removal of ibuprofen from aqueous solution: a non-catalytic and catalytic ozonation study in a semi-batch reactor. Appl. Catal. B Environ. 230, 77–90. https://doi.org/10.1016/j.apcatb.2018.02.021.
Shang, Y., Chen, C., Zhang, P., Yue, Q., Li, Y., Gao, B., Xu, X., 2019. Removal of sulfamethoxazole from water via activation of persulfate by Fe3C@NCNTs including mechanism of radical and nonradical process. Chem. Eng. J. 375, 122004. https://doi.org/10.1016/j.cej.2019.122004.
Shi, P., Su, R., Zhu, S., Zhu, M., Li, D., Xu, S., 2012. Supported cobalt oxide on graphene oxide: highly efficient catalysts for the removal of Orange II from water. J. Hazard Mater. 229–230, 331–339. https://doi.org/10.1016/j.jhazmat.2012.06.007.
Sousa, J.C.G., Ribeiro, A.R., Barbosa, M.O., Pereira, M.F.R., Silva, A.M.T., 2018. A review on environmental monitoring of water organic pollutants identified by EU guidelines. J. Hazard Mater. 344, 146–162. https://doi.org/10.1016/j.jhazmat.2017.09.058.
Southichak, B., Nakano, K., Nomura, M., Chiba, N., Nishimura, O., 2006. Phragmites australis: a novel biosorbent for the removal of heavy metals from aqueous solution. Water Res. 40, 2295–2302. https://doi.org/10.1016/j.watres.2006.04.027.
Sun, B., Ma, W., Wang, N., Xu, P., Zhang, L., Wang, B., Zhao, H., Lin, K.-Y.A., Du, Y., 2019. Polyaniline: a new metal-free catalyst for peroxymonosulfate activation with highly efficient and durable removal of organic pollutants. Environ. Sci. Technol. 53, 9771–9780. https://doi.org/10.1021/acs.est.9b03374.
Swarnalatha, K., Ayoob, S., 2016. Adsorption studies on coir pith for heavy metal removal. Int. J. Sustain. Eng. 9, 259–265. https://doi.org/10.1080/19397038.2016.1152323.
Tan, C., Gao, N., Deng, Y., Zhang, Y., Sui, M., Deng, J., Zhou, S., 2013. Degradation of antipyrine by UV, UV/H2O2 and UV/PS. J. Hazard Mater. 260, 1008–1016. https://doi.org/10.1016/j.jhazmat.2013.06.060.
Teppor, P., Jäger, R., Paalo, M., Palm, R., Volobujeva, O., Härk, E., Kochovski, Z., Romann, T., Härmas, R., Aruväli, J., Kikas, A., Lust, E., 2020. Peat-derived carbon-based non-platinum group metal type catalyst for oxygen reduction and evolution reactions. Electrochem. Commun. 113, 106700. https://doi.org/10.1016/j.elecom.2020.106700.
Tian, W., Zhang, H., Qian, Z., Ouyang, T., Sun, H., Qin, J., Tadé, M.O., Wang, S., 2018. Bread-making synthesis of hierarchically Co@C nanoarchitecture in heteroatom doped porous carbons for oxidative degradation of emerging contaminants. Appl. Catal. B Environ. 225, 76–83. https://doi.org/10.1016/j.apcatb.2017.11.056.
Vijayaraghavan, K., Yun, Y.-S., 2008. Bacterial biosorbents and biosorption. Biotechnol. Adv. 26, 266–291. https://doi.org/10.1016/j.biotechadv.2008.02.002.
Wang, J., Wang, S., 2018. Activation of persulfate (PS) and peroxymonosulfate (PMS) and application for the degradation of emerging contaminants. Chem. Eng. J. 334, 1502–1517. https://doi.org/10.1016/j.cej.2017.11.059.
Wang, S., Shan, R., Gu, J., Zhang, J., Zhang, Y., Yuan, H., Chen, Y., Luo, B., 2020. Reactivity and deactivation mechanisms of toluene reforming over waste peat char-supported Fe/Ni/Ca catalyst. Fuel 271, 117517. https://doi.org/10.1016/j.fuel.2020.117517.
Wang, Y., Shen, C., Li, L., Li, H., Zhang, M., 2016. Electrocatalytic degradation of ibuprofen in aqueous solution by a cobalt-doped modified lead dioxide electrode: influencing factors and energy demand. RSC Adv. 6, 30598–30610. https://doi.org/10.1039/C5RA27382J.
Williams, N.S., Ray, M.B., Gomaa, H.G., 2012. Removal of ibuprofen and 4-isobutylacetophenone by non-dispersive solvent extraction using a hollow fibre membrane contactor. Separ. Purif. Technol. 88, 61–69. https://doi.org/10.1016/j.seppur.2011.11.022.
Xiang, Y., Fang, J., Shang, C., 2016. Kinetics and pathways of ibuprofen degradation by the UV/chlorine advanced oxidation process. Water Res. 90, 301–308. https://doi.org/10.1016/j.watres.2015.11.069.
Xie, W., Weng, L.-T., Ng, K.M., Chan, C.K., Chan, C.-M., 2017. Defects of clean graphene and sputtered graphite surfaces characterized by time-of-flight secondary ion mass spectrometry and X-ray photoelectron spectroscopy. Carbon 112, 192–200. https://doi.org/10.1016/j.carbon.2016.11.002.
Yanan, S., Xing, X., Yue, Q., Gao, B., Li, Y., 2020. Nitrogen-doped carbon nanotubes encapsulating Fe/Zn nanoparticles as a persulfate activator for sulfamethoxazole degradation: role of encapsulated bimetallic nanoparticles and nonradical reaction. Environ. Sci. Nano 7, 1444–1453. https://doi.org/10.1039/D0EN00050G.
Yang, S., Wang, P., Yang, X., Shan, L., Zhang, W., Shao, X., Niu, R., 2010. Degradation efficiencies of azo dye Acid Orange 7 by the interaction of heat, UV and anions with common oxidants: persulfate, peroxymonosulfate and hydrogen peroxide. J. Hazard Mater. 179, 552–558. https://doi.org/10.1016/j.jhazmat.2010.03.039.
Yang, Y., Banerjee, G., Brudvig, G.W., Kim, J.-H., Pignatello, J.J., 2018. Oxidation of organic compounds in water by unactivated peroxymonosulfate. Environ. Sci. Technol. 52, 5911–5919. https://doi.org/10.1021/acs.est.8b00735.
Zhang, G., Ding, Y., Nie, W., Tang, H., 2019. Efficient degradation of drug ibuprofen through catalytic activation of peroxymonosulfate by Fe3C embedded on carbon. J. Environ. Sci. 78, 1–12. https://doi.org/10.1016/j.jes.2018.10.002.
Zhong, H., Duan, L., Ye, P., Li, X., Xu, A., Peng, Q., 2019. Synthesis of cobalt–nitrogen-doped mesoporous carbon from chitosan and its performance for pollutant degradation as Fenton-like catalysts. Res. Chem. Intermed. 45, 907–918. https://doi.org/10.1007/s11164-018-3655-y.